ARPN Journal of Engineering and Applied Sciences


www.arpnjournals.com

# EFFECT OF NUMBER OF TRIGGERS AND SHAPE OF CRASH BOX ON ENERGY ABSORPTION DURING EXPERIMENTAL COLLISION

Ahmad Yunus Nasution[1,2], Mohd Ruzaimi Mat Rejab[1], Januar Parlaungan Siregar[1] and Quanjin Ma[1]
[1]Faculty of Mechanical and Automotive Engineering Technology, University Malaysia Pahang, Pekan, Pahang, Malaysia
[2]Mechanical Engineering Department, Engineering Faculty, Universitas Sumatera Utara, Jl. Dr. T. Mansur, Medan, Sumatera Utara, Indonesia
E-Mail: ahmadjunusa@usu.ac.id

**ABSTRACT**

The capacity of passenger car crash boxes to absorb energy during crashes has been the subject of extensive research, which started with the creation of multiple crash box models, changes in crash box filling, and the inclusion of crash box triggers. On the other hand, no research has been done on the combination of axle trigger holes, nine-cell columns, and crash box models. The results of the experiment on the energy-absorbing capacity of AA6061-T4 crash box specimens under compressive loads are presented in this paper. The compression tests were conducted on a Universal Testing Machine with a maximum force capability of 1000 kN and a speed capability of 5 mm/s. Three models are used in crash box modeling. A cross-section of the model with a round hole-shaped trigger variation is included in these three versions. It is established that the hexagonal Frusta type with two holes absorbs the highest energy at 33.30 kJ, and has a displacement of 4.12 mm and a maximum force of 348.5 kN. The energy absorption capacity of the crash box was found to be increased by combining frusta versions of the hexagon model with two holes and nine-cell column filling.

**Keywords:** crash box; frusta model; trigger circle; nine-cell column.

Manuscript Received 4 March 2024; Revised 18 June 2024; Published 10 August 2024

## 1. INTRODUCTION

A crash box is made to take in impact energy and store it. The purpose of the crash box is to shield the primary vehicle and its occupant structures from more serious harm [1]. Because of the high global accident rate, crash box innovation has drawn a lot of attention in the last 10 years and is considered a significant development in the automotive industry. They can reduce the force and damage that collides with other parts [2]. This study generated a crash box design approach that used a frustra-shaped model with a trigger circle and a cross-section that was optimized for energy absorption during compression testing [3]. The experiments were conducted using compression testing and experimental analysis to assess how well the crash box dispersed the load and absorbed energy [4]. The trigger ring and crash box's cross-section are designed to improve the device's capacity for load distribution and energy absorption. The experimental study also clarifies the collision box's deformation behavior, which is crucial for assessing how effective it is at lessening the force of a collision [5].

A number of crash box models, first in the forms of a box, hexagon, and circle have been used for research and applications [6]. Additionally, shapes like boxes, hexagons, and circles are created by combining the shaft components with triggers. In addition, these triggers are available in a range of forms, such as square holes, hexagons, circles, and welding triggers [7]. Different crash box structural models determine how the material deforms in a crash and can also be customized for a certain material to get the best overall efficiency, which is often defined by specific energy absorption [8]. Currently, available options for this crash box's contents include aluminum foam filling, filler, and filling composed of aluminum material itself. The shapes of the filling model were also changed, starting with the hexagon, star, square, cross-section, and honeybeam forms [9].

According to earlier studies, the multicell crash box design outperforms the single-cell crash box design in terms of energy absorption capacity and peak forces [10]. By effectively distributing impact loads among cells, the multicell design may provide more gradual deformations and a higher energy absorption capacity [11], One may classify the single-cell structure as a classic design [12]. When compared to circular and hexagonal tubes in the crash box, square-shaped tubes exhibited the highest energy absorption capacity and the lowest peak forces [13]. Additionally, the rectangular tube exhibits more predictable and controlled deformation behavior, making it the better choice in collision scenarios. The impact performance of the round and hexagonal tubes is still good, though. This research provides insight into the relationship between tube shape and crash performance, enabling designers to produce impact boxes that are safer and more efficient. This study also highlights how important it is to use aluminum for crash boxes because of its high energy absorption capacity and lightweight [14]. The energy absorption capacity, initial peak force, deformation modes, and protective qualities of the original and modified crash boxes were assessed using compression tests [15]. The stability of the ongoing deformation following the first buckling is influenced by the triggers, the crash-box length, and the cross section. It is evident from all of the research that has been done that no single study project carried out by earlier scholars merged the entrance, trigger crash box, and model. Since it significantly affects the amount of energy absorbed

during a collision, completing this is essential. Therefore, the goal of this work is to combine cross-section entries with three crash box models-the square, hexagon, and circle-and provide a circle-shaped trigger for the circle-shaped shaft crash box. The goal of combining these three features into a single crash box model is to improve the crash box's capacity to absorb energy during a collision. Aluminum AA was used by the researchers in order to promote buckling in the crash box.

## 2. METHODS

### 2.1 Aluminium AA 6061

The height of the wall was AA6061, with a range of 0.794 mm to 3.175 mm. The observed force responses to tensile tensions ranged from 85% to 92%. The mechanical parameters of other, more well-known tensile energy dissipation solutions were significantly less than the measured energy absorption values, which ranged from 2.2 kJ to 7.7 kJ and 12 kJ/kg to 16 kJ/kg for specific energy absorption. During testing, the majority of specimen types showed fairly uniform and homogenous deformation [16].

Owing to its availability in numerous forms, including sheets, plates, bars, tubes, and extrusions, AA 6061 is a very adaptable material that may be utilized in a multitude of applications. As seen in Table-1, its outstanding strength-to-weight ratio, resistance to corrosion and ease of manufacturing make it a popular material for consumer goods and architectural applications. It is also a great option for structural parts used in the aerospace and automotive industries [17].

**Table-1.** Mechanical properties AA6061.

| Mechanical Property | Typical Value | Unit |
|---|---|---|
| Shear Strength | 207 - 240 | MPa |
| Poisson's Ratio | 0.33 | |
| Density | 2.7 | g/cm³ |
| Melting Point | 582 - 652 | °C |
| Specific Heat Capacity | 0.897 | J/(g·°C) |
| Thermal Conductivity | 151 - 202 | W/(m·K) |
| Coefficient of Thermal Expansion | 23.2 x 10^-6 | 1/°C |
| Electrical Conductivity | 47 - 59 | MS/m |

Silicon: 0.4-0.8%, copper: 0.15-0.4%, magnesium: 0.8-1.2%, iron: less than 0.7%, zinc: less than 0.15%, chromium: less than 0.25%, manganese: less than 0.15%, and titanium: less than 0.05% are the compositions of aluminum AA 6061. Tensile strength of aluminum alloy AA 6061 is 45,000-65,000 psi (310-450 MPa), and yield strength is 40,000-55,000 psi (275-380 MPa). Its exceptional ductility allows it to be shaped into intricate shapes without breaking apart. Because of its great machinability, aluminum is easy to mold, drill, and cut using conventional machining techniques. Additionally, it welds well with a variety of welding techniques, including gas welding, MIG, and TIG [10]. It's crucial to keep in mind that in order to stop cracking, preheating and post-weld heat treatment can be necessary. Because of this chemical's strong resistance to corrosion in a range of conditions, including saltwater, it is frequently employed in nautical applications. Its resistance to corrosion is inferior to that of other aluminum alloys, such AA 7075. The final material is aluminum, which is frequently utilized in products including electrical connections, bicycle frames, car parts, and building and bridge structural components. It is also frequently utilized in the manufacturing of consumer items, like as smartphone cases, sports equipment, and PCs.

### 2.2 Design Process

In designing a crash box, the first thing to do is make a design. The first design model is made using Solidworks software as in Figure-1. In this Solidworks software, the model is made in isometric form and has front, top, bottom and side views. For the dimensions themselves, because the crash box is in the form frusta, the upper and lower bases have different dimensions. The upper base is 60 mm, the lower base is 100 mm, and the length is 100 mm. The reason for choosing Solidworks software is because it has easier design capabilities and can import and export in different formats so that it is easy to apply to the next software [18].

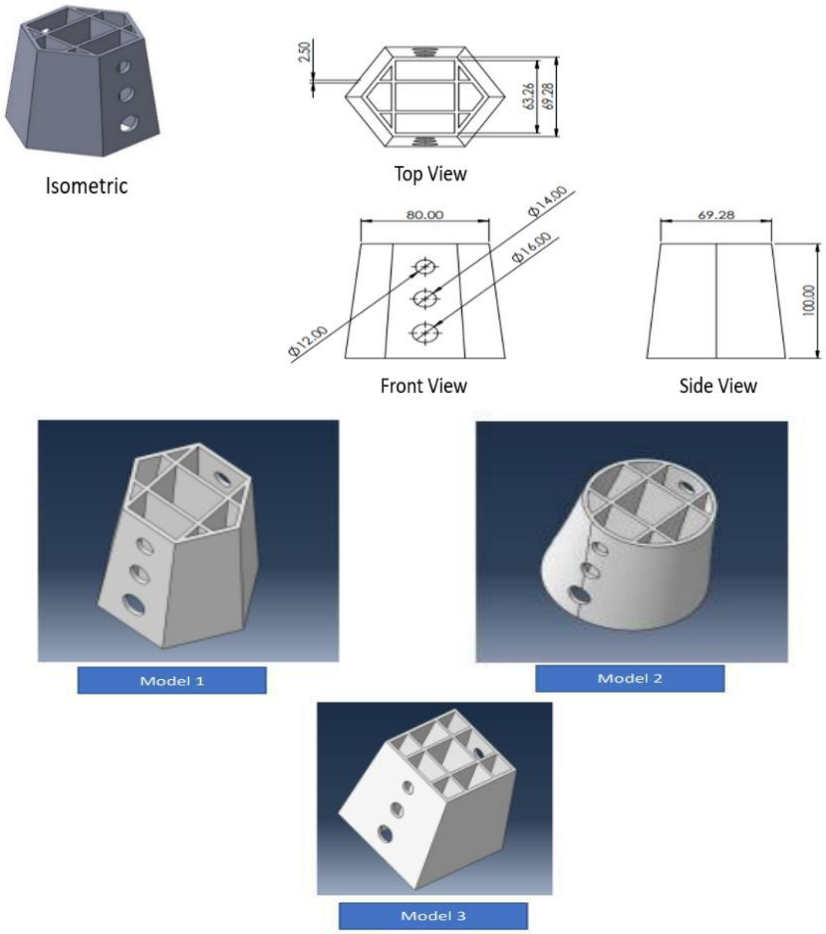


**Figure-1.** Sample of crash box design result.

This study made nine crash box specimens with three different models. The first model was the frusta circle model with cross-section filling, where each model varied the trigger, namely one hole, two holes, and three holes. The second model was the frusta hexagon model, and the third model is the frusta square model. For these three models, the difference is the triggers for each model. By providing trigger variations for each crash box model, it is hoped that the maximum force value will be obtained so that the energy absorption that the crash box can carry out is known [19]. Positions of the triggering holes in the crash box are set 20 mm from the middle of the center hole, and then two holes become from the upper and bottom with a space of 20 mm also.

According to studies by Mirosaw Ferdynus (2022), due to its benefits over circular or parallelepiped tubes (lowering the peak crushing force and stabilizing the crushing process), Frusta is employed as a crash box, absorbing the energy of the impact load in the collision [20]. Columns with one, three, or five holes positioned at a line 30 mm from the base were examined based on the findings of earlier investigations. The usage of holes has a favorable impact on the chosen crushing characteristics, according to numerical analyses that are supported by bench-scale experimental tests [21]. Multicell columns are becoming increasingly attractive in crashworthiness applications because of their high material-use efficiency. Meanwhile, there is an urgent need to develop new structures to achieve the goal of lightweight without compromising crashworthiness. multicell columns with nine-cell columns show a competitive advantage over uniform columns as energy absorbers [22].

This is what underlies the researchers' decision to combine the frusta model crash box design with nine-cell columns and variations of circle-shaped triggers to get a crash box that has a lightweight material but can absorb large amounts of energy.

### 2.3 Manufacturing Process

Images from the crash box generation procedure are displayed in Figure-2. The first step in the procedure is to prepare the AA6061 material into a roll. To create the specimen in accordance with the design, the material is next cut and shaped. Finally, welding and polishing are completed.

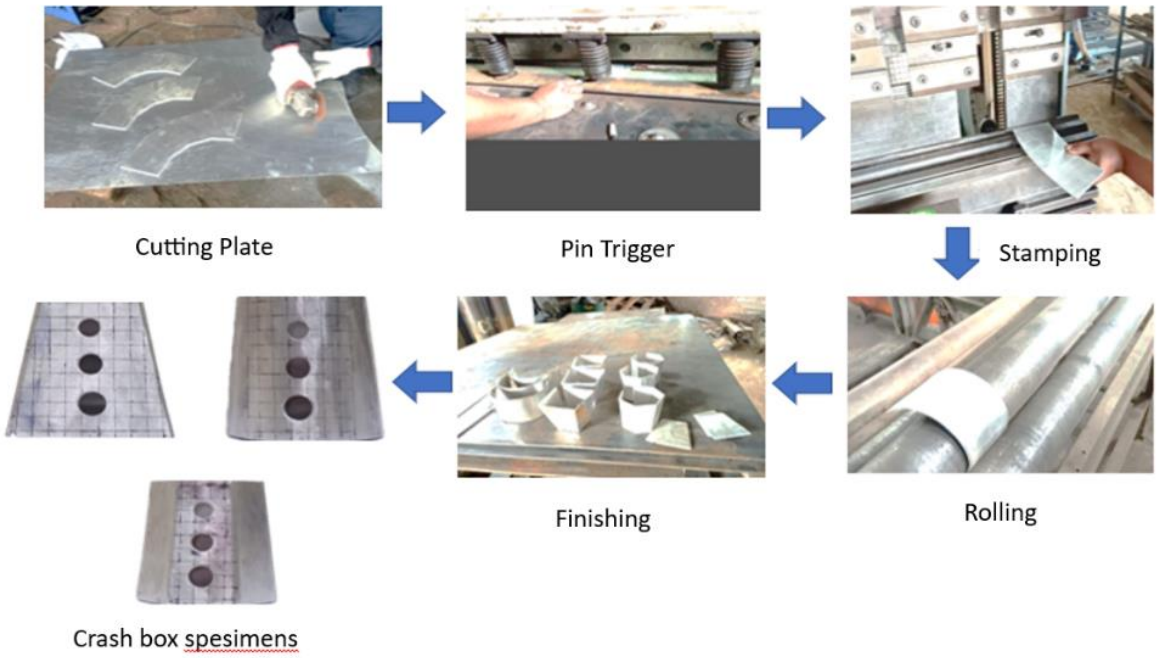


**Figure-2.** Manufacturing process.

The acquisition of AA 6061-T4 material sheets is the first step in the crash box production process, which culminates in the manufacture of the crash box itself. First, use the AA 6061-T4 material sheet to make the crashbox shape. After sketching, the sheet material is cut into pieces. The most important item or equipment to prepare for plate cutting is a hand grinder, as well as a thick iron or aluminum ruler. The first step is to draw a cut line on the surface of the plate with a permanent marker on both sides. Then, make scratches on both sides with a cutter knife, an iron ruler, and/or a water pass.

After the material is cut into pieces, holes or pins are made. There are numerous methods for making holes in manufactured items. One technique that is often used is punching. The process of punching holes in work materials using press dies is called punching. Press dies are made up of presses known as punches and molds known as dies. The next step is stamping, which involves forming the aluminum sheet with a stamping machine. A stamping machine, also known as a stamping press, is a machine that shapes or cuts metal, plastic, or other materials with a stamping die. The next stage is rolling. Based on the geometry of the workpiece, this rolling process is carried out to reduce the thickness of the box-shaped workpiece. In this rolling process, the workpiece with a box-shaped cross section is converted into a product with a particular shape/profile.

The produced material is then fused between the edges of the shell using TIG welding. The material that has been produced and joined by TIG welding is called tungsten inert gas (TIG) welding. Tungsten electrodes-non-consumable tungsten are used in the Tungsten Inert Gas (TIG) welding technique. A gas covering (typically argon/helium gas or a combination of both) shields and covers the welding area. Because it is heavier than air and produces superior welding coverage areas, argon is frequently utilized in welding.

### 2.4 Compression Test

One common technique for assessing the strength and deformation properties of materials-especially those used in crash boxes-is compression testing. The Shimadzu 1000 KN Universal Testing Machine, with a five mm/s velocity and capacity, is depicted in Figure-3. Techniques for compression testing were governed by the American Society for Testing and Materials (ASTM) E9-19 Standard Test Methods of Compression Testing. The material's deformation, compressive strength, and modulus of elasticity are the test's parameters. These properties allow for the calculation of the absorbed energy. Nine specimen samples made of aluminum AA 6061-T4 were used in the test; the samples included variations of three circle models, three hexagon models, and three square models.

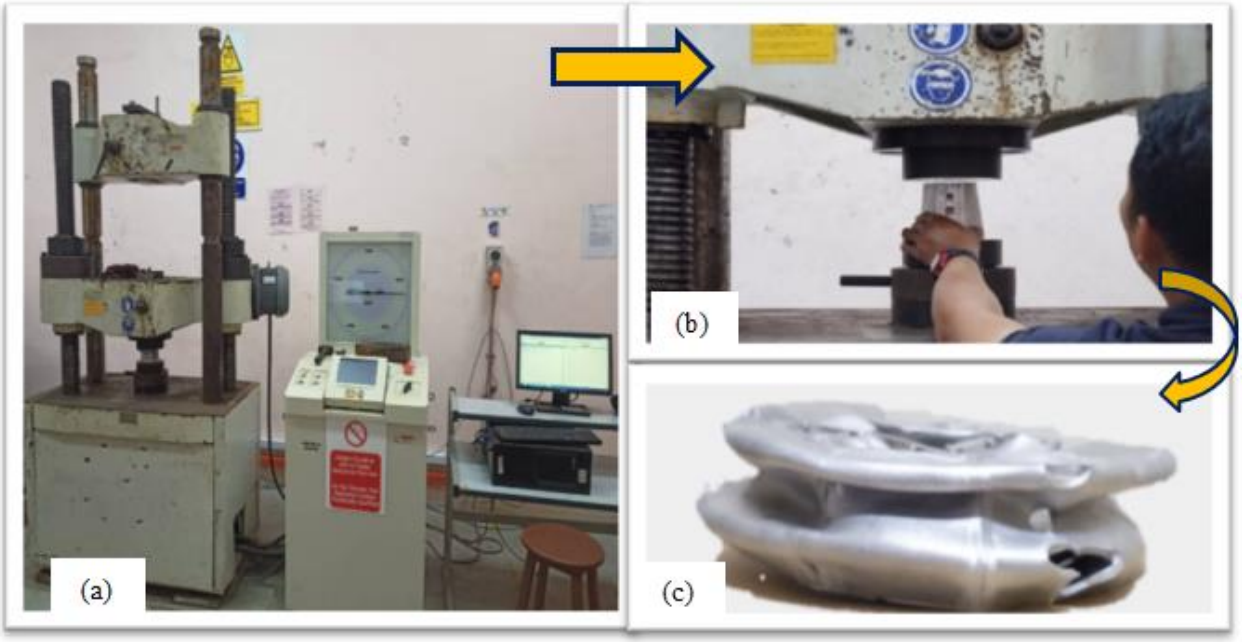


**Figure-3.** Compression test process (a. Universal testing machine; b. Process compression; c. Result of compression test.)

A sample of crash box material is regularly put through compression testing to evaluate its mechanical characteristics. First, the sample is made according to the specifications that correspond to the real component's dimensions and shape. After the sample is ready, it is put on a compression testing device that has been calibrated in accordance with the necessary guidelines and standards [23]. The sample is continuously compressed until the point of total compression or until a predetermined deformation or failure point is reached in order to perform the compression test. Among other mechanical parameters, the material's elastic modulus, compressive strength, and yield strength are ascertained by gathering and evaluating the load and deformation data from the test. Next, by contrasting these values with the relevant requirements and standards, it will be possible to ascertain whether the material satisfies the essential criteria [24].

The load-deformation curve calculated mechanical parameters, and any significant notes or observations regarding the testing methodology or sample preparation are all included in the compression test results report and are all presented in a standard manner. This method allows researchers and engineers to precisely examine the mechanical characteristics of crash box materials to make sure they are suitable for the intended function [25].

## 3. RESULT AND DISCUSSIONS

Figure-4 shows how the compression engine unit was immediately connected to a monitor on the Universal testing machine, which used a camera as a tool to monitor the compression results.

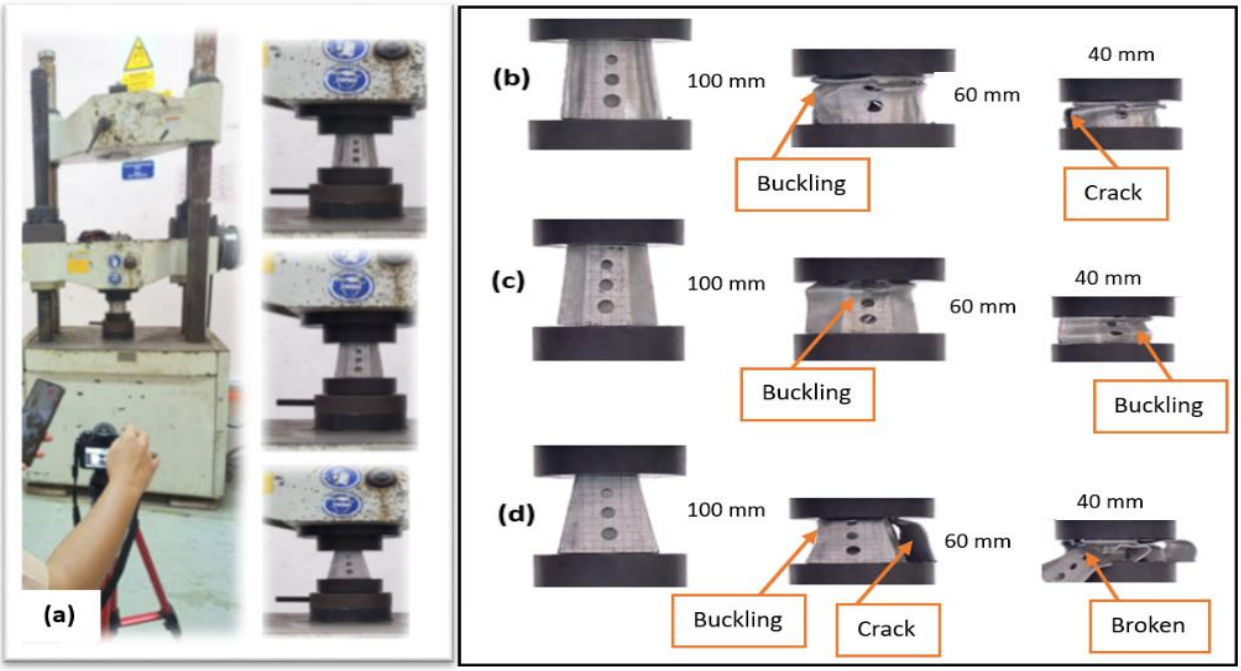


**Figure-4.** Compression test: (a) Compression test using the universal testing machine; (b) Circle compression result; (c) Hexagon compression result; (d) Square compression result.

The researchers used a universal testing apparatus with a 1000 KN capacity and a 5 mm/s velocity to test the crash box specimens. The researcher uses an SLR camera to record the moment of deformation and buckling when testing the crash box using the Universal Testing Machine (Figure a). Based on the findings of the earlier Abaqus test, which showed that the maximum force result was more than 500 kN, this machine was selected. The crash box specimen's deformation is depicted in Figure-4. This is in line with predictions: the crash box specimen, which is not damaged, experiences deformation and buckling. The manufacturing process is the basis for this experiment.

Figure-4 (b) is a crash box model circle with an initial length of 100 mm, and the pressure is applied to the crash box. This shows that buckling started at the base of the crash box before the first hole. Figure-4 (b) also shows a crack in the crash box, and this occurs in the crash box section, which is in welding due to the inability of the welding part to withstand the applied load [26]. Figure-4 (c) is a hexagon model crash box. In Figure-4 (c), it can be seen that buckling occurs starting from the initial given pressure until the final length reaches 40 mm. In this model, there is no crack, which shows that the hexagon model is stronger to withstand loads even though it has a broader welding area, the same as the circle model [27]. Figure-4 (d) is a crash box model square. In the figure it can be seen that in addition to buckling, there is also a crack from the beginning when the pressure is applied to the end of the pressure. Even in this model, the shape part is damaged on all sides of the crash box. So that only the filling is holding the pressure load, the crash box is in the form of nine-cell columns. This is probably caused by errors during manufacturing and welding is an imperfect welding process so that the welded part is exposed when pressure is applied [28].

Testing experimentally using a 1-hole trigger variant on a crash box indicates that the hexagon model has a higher force value than the other two types. Comparably, the hexagon type with a single shaft hole performs better than the square and circular models in terms of the crash box's capacity to absorb energy.

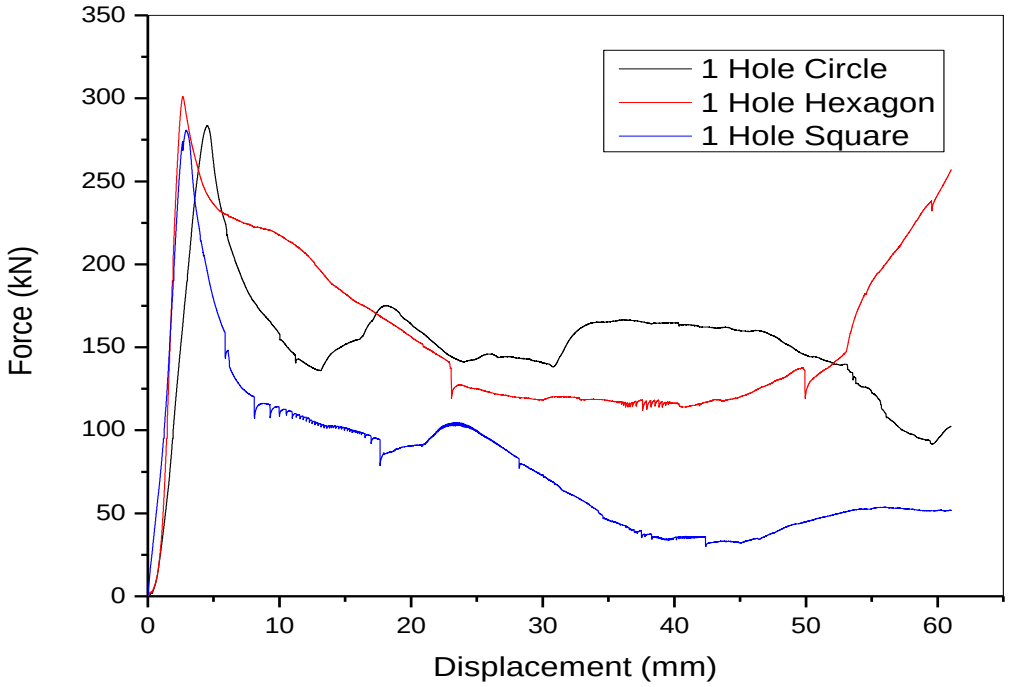


**Figure-5.** Force value on displacement result from one hole.

The maximum force values for the three types of crash boxes do not differ substantially, as shown in Figure-5. At a displacement of 2.63 mm, the force value for the hexagon model is 298.64 kN. The circular model has a maximum force of 283.51 kN, which is greater than the square model's 279.40 kN and 3.57 mm displacement. and a 4.53 mm displacement. The graph shows that there are no appreciable differences between the maximum force values for any of the models. The hexagon model has the largest maximum force value when compared to other models since it has six supports that can support the maximum load when applied. This is because each model only has one hole as a trigger, which means that deformation occurs gradually [8].

Figure-6 depicts a displacement-force comparison on a crash box with two shaft openings. According to the test results, the hexagon, square, and circle models had the most significant displacement and highest force.

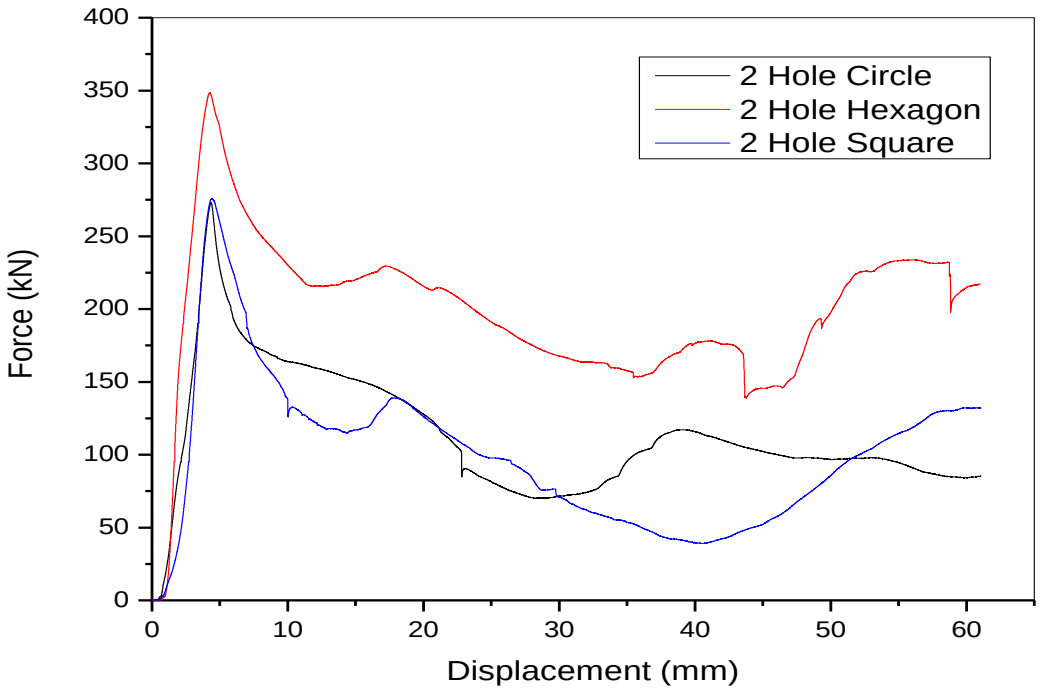


**Figure-6.** Force value on displacement result from two hole.

The hexagon model's maximum force value, as seen in Figure-6, is 347.95 kN at a displacement of 4.19 mm. This proves the hexagon-shaped currency box model with the two trigger holes can support the specified weight. The maximum force values of the other two models, however, deviate considerably from the hexagon model. Apart from this model, the square model (maximum force of 275.05 kN with displacement of 5.03 mm) and the circle model (maximum force of 271.32 kN with displacement of 4.26 mm) are affected by the number of holes in the shaft crash box. The hexagon is displayed in this graph. The hexagon model has six supports in its shape when it gets a load, which is why the model with two holes has the largest maximum force value. The crash box's high cross section increases the box's ability to crash when loaded by contributing to the highest maximum force value. The two-hole hexagon model has a higher maximum force value than the one-hole hexagon model, but since a one-hole hexagon only has one trigger, it is evident that the maximum force value of one hole is greater than the maximum force value of two holes. [29].

The cross-section and a trigger circle with three holes were used to test the square, hexagonal, and circle crash box models. The findings are shown in Figure 7. A comparison of displacement and force is shown in the graph. According to the graph above, at a displacement of 5.17 mm, the hexagon model with the greatest force generates 325.35 kN. With a displacement of 4.13 mm and a force value of 274.5 kN, the square model has the second-highest force value, trailed by the circular model's 244.15 kN and 4.20 mm displacement.

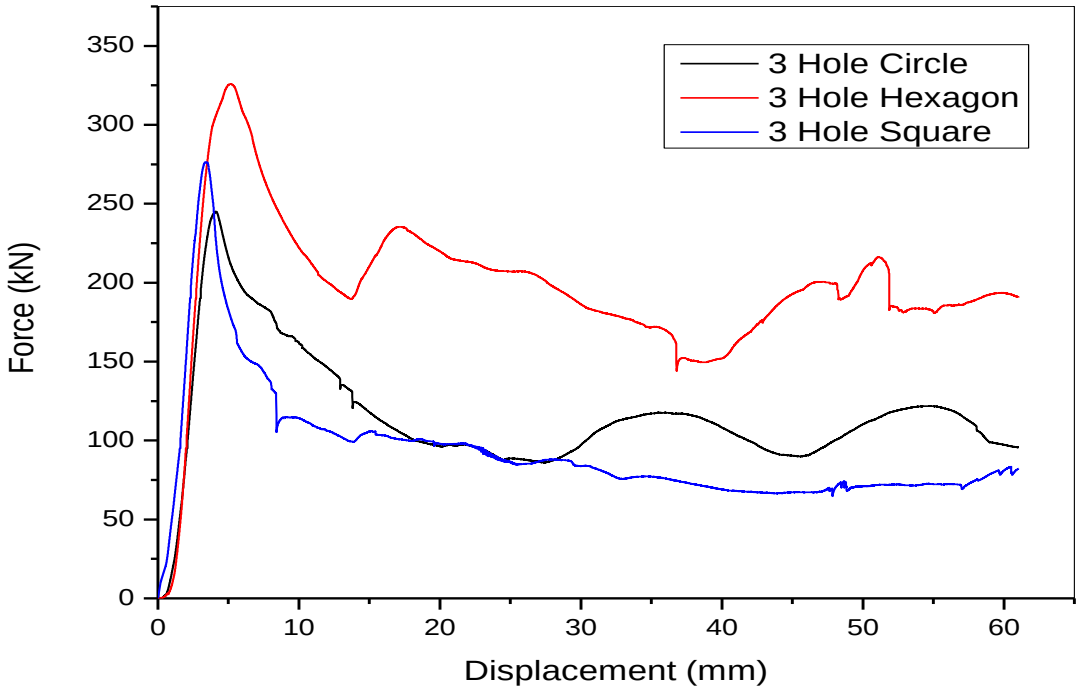


**Figure-7.** Force value on displacement result from three holes.

As seen in Figure-7, the maximum force of the hexagon model is greater than that of the square and circle models. Comparably, the displacements in the three models show that the hexagon model has a sizable displacement value, suggesting that during experimental testing, the hexagon model absorbs a sizable quantity of energy. Compared to the two-hole version, the three-hole hexagon model has a lower maximum force value Nevertheless, the hole is greater than one. This is a result of the forces applied to the crash box that are proportionate to the size of each existing hole. Similar to the previous two models, the hexagon variant including three holes offers a greater maximum force value. This is produced by the cross-section's existence as well as the shape's six supports and the crash box's actual contents [30].

The energy absorption values of all the models differ considerably, as Figure-8 shows, but the hexagon model has the maximum energy absorption of all the models. The two-hole energy absorption in the hexagon model is 33.30 kJ. In the square form, the two-hole energy absorption is 28.23 kJ, while in the circle model it is 27.83 kJ.

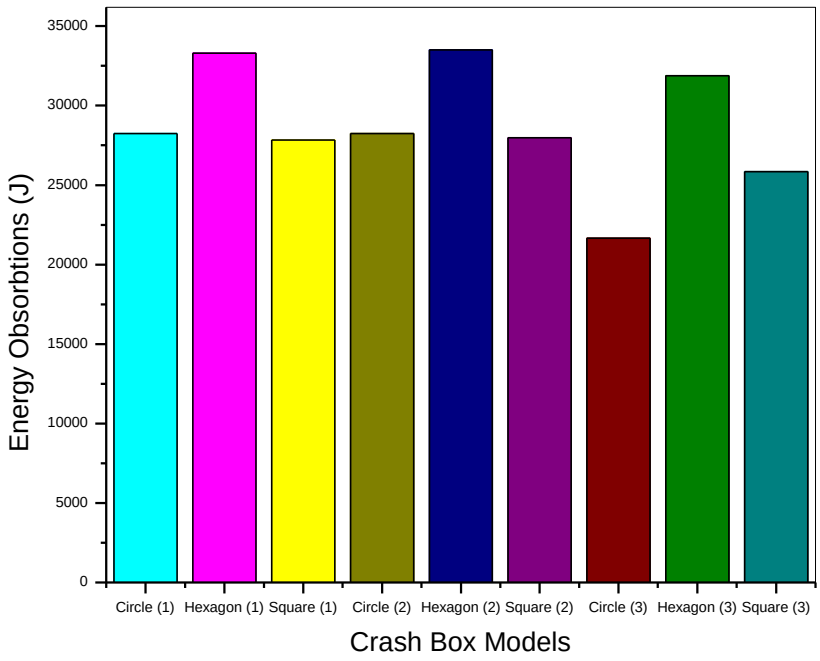


**Figure-8.** The energy absorption value for each model.

The relationship between the maximum force value in each crash box model and the crash box's energy absorption value is shown in Figure-8. The quantity of energy absorbed by the crash box increases with its maximum force. Additionally, this graph demonstrates that when a load is applied, the hexagon crash box model absorbs the greatest energy. This is due to the six sides of the hexagon model's ability to withstand pressure loads. The graph also demonstrates that two holes are the maximum number of triggers that can produce force. This is due to the fact that the crash box's cross-sectional area decreases with the number of holes. The crash box's capacity to withstand small loads and absorb energy consequently declines.

A crash box is a dispersible kinetic energy-dispersing deformable object. The Crash Box needs to have the capacity to collapse before other body parts in order to absorb crash energy during a collision, lessen damage to the main cabin frame, and save passenger lives. To reduce vehicle damage, the crash box must experience plastic deformation before other components. The ability of automotive components to absorb energy during collision is commonly measured by their energy absorption. To shield the occupants from abrupt bursts of high acceleration, a high force indicates a strong absorption of energy, although it is preferable for this to happen over extended durations. As a result, there is consistent energy absorption throughout time, which raises the crash force efficiency. There are at least two different types of energy absorption management in front of the vehicle. As the initial component to absorb collision energy, the crash box deforms structurally, with buckling emerging as the primary feature [31].

The thin wall prismatic column, device shape at the front rail, material thickness, cross-section dimensions, structural material used in manufacture, and connection mechanism used all affect how effective the devices are [31]. For optimizing the design of the crash box, namely, to obtain high energy absorption, such as the type of splicing during part assembly and the typical materials used in the design and to reduce the accident rate that can cause material loss and even death during a construction accident incident. Figure-9 describes the vehicle safety system. This structure is essential for vehicle front-end energy absorption and occupant protection during low-velocity frontal collisions. It consists of the bumper, the reinforced plate behind the bumper, the inner and outer parts of the crash box, the inner and outer parts of the front rail, the fixed plate that fixes the front rail's end constraint, and the connection. To further enhance design, many blocks of foam filler are positioned inside the crash box and bumper. As illustrated in Figure-9, the proper energy transfer path is for the bumper to transfer energy to the left and right crash boxes, causing the crash box to compress and allowing force to pass to the front rail through the connecting plate.

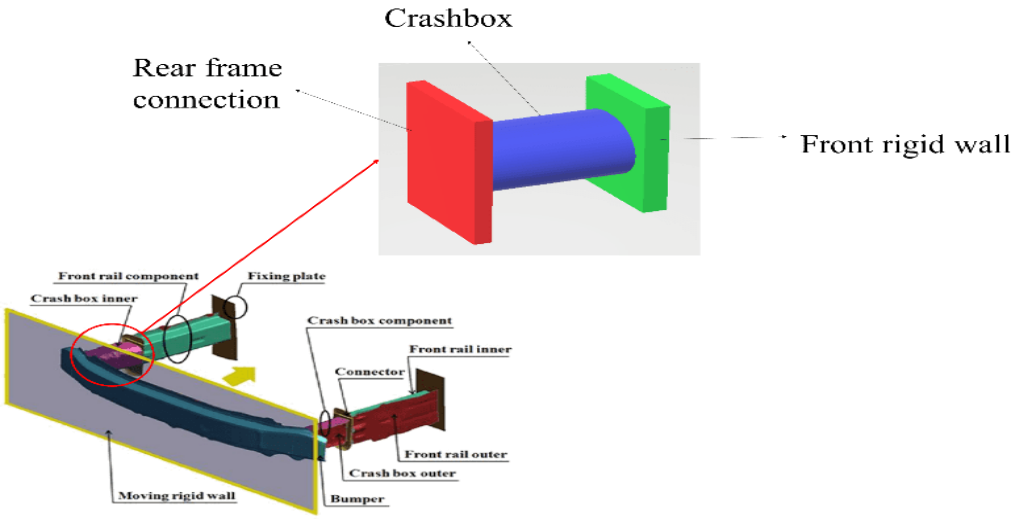


**Figure-9.** Front end structure of the automobile equipped with components of the crash box.

The front end structure of the car, which includes the front rail and a component crash box, is seen in Figure-9. If the impact kinetic energy is less than the crash box's energy absorption limit, the front rail will be effectively protected; if not, it will be damaged by a significant deflection and a significant collision force that is transferred to the passenger compartment. After a low-speed collision, replacing a bumper or crash box is very inexpensive, but fixing a front rail is very expensive [32]. An illustration of the force flow diagram when a collision occurs over time is depicted in Figure-10.

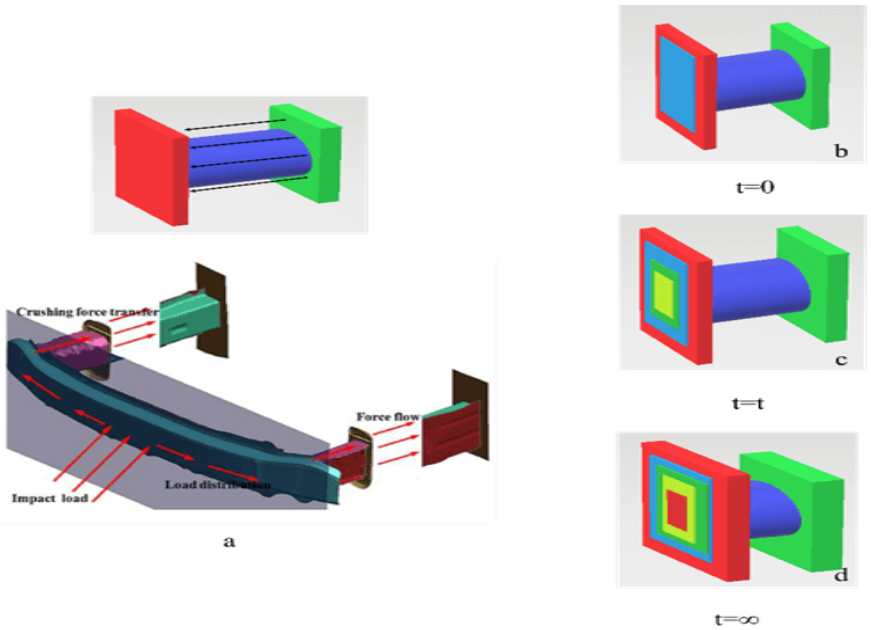


**Figure-10.** Force flow diagram when the collision occurred over time that happened in the contour crash box.

The contour crash box's force flow diagram is displayed in Figure-10 during a collision. The front end structure shown in Figure-10a is optimal because it prevents excessive lateral bending or instability in the deflection, which could cause the front structure to crumple sharply and encroach on the occupants' residual space, while also shielding the front rail from significant deformation in the event that the crash box is crushed. The front rail's compressive deformation should, as much as feasible, occur in the axial direction [33]. Figure-10b-d illustrates the contour impact condition of the rear frame connection when the collision occurred over time. In the condition at the time t = 0, which is the initial state of the cross-section, it indicates that no collision has occurred, and the blue color represents the minimum compressive force obtained spread over the cross-section. At the time of the t = t condition, the

collision begins to occur within a certain period of time, and there is already a stronger variation in the distribution of compressive forces indicated by the addition of green and yellow colors. Finally, at the time of t=t∞, the collision condition has the highest impact on the cross-sectional contour, which provides the maximum compressive force shown in red so that the crash box so that the event explains the occurrence of buckling, crack, and break in the crash box.

## 4. CONCLUSIONS

Experiments were conducted on a variety of crash box test items, such as cross section filled or nine-cell columns with three-hole trigger rings, as well as circular, hexagonal, and square models. The hexagon model absorbs the greatest energy, 33.30 kJ, with a force of 348.5 KN at a displacement of 4.12 mm, according to test findings from a universal testing machine with a 1000 KN capacity and a speed of 5 mm/s. It may be deduced that adding filler to crash boxes in the shape of cross sections and triggers enhances the crash box's capacity to absorb energy under load. The maximal force value of the crash box is directly proportional to its energy absorption value. There is a restriction of two holes in the crash box shape, however holes can cause buckling. It is evident that a three-hole trigger has a lower energy absorption value than a two-hole trigger. The course of future research will involve some optimization based on the results of the experiments.

**Funding**

The study was funded by Universiti Malaysia Pahang under grant number PGRS210340, for which the authors are appreciative. SUPREME Focus Group, who supplied the tools and materials for the research, has generously sponsored this effort.

## ADDITIONAL INFORMATION

The datasets created and/or analyzed for this study are not available to the general public because they are all the result of ongoing PhD research and cannot be accessed by the public until the final PhD thesis is completed and submitted. However, the corresponding author can provide the datasets upon reasonable request.

## REFERENCES

[1] H. Yin, L. Zhang, Z. Liu, W. Fan, X. Wu and G. Wen. 2023. Crash analysis and evaluation of a new separate W-beam guardrail on highways using the finite element method. Eng. Struct., vol. 278, doi: 10.1016/j.engstruct.2022.115551.

[2] R. Yang *et al*. 2019. Safety effects of street lighting on roadway segments: Development of a crash modification function. Traffic Inj. Prev., 20(3): 296-302, doi: 10.1080/15389588.2019.1573317.

[3] P. C. Arunakumara, H. N. Sagar, B. Gautam, R. George and S. Rajeesh. 2023. A review study on fatigue behavior of aluminum 6061 T-6 and 6082 T-6 alloys welded by MIG and FS welding methods. Mater. Today Proc., 74: 293-301, doi: 10.1016/j.matpr.2022.08.242.

[4] D.Gao, S. Wang, M. Zhang and C. Zhang. 2021. Experimental and numerical investigation on in-plane impact behaviour of chiral auxetic structure. Compos. Struct. 267: 113922, doi: 10.1016/j.compstruct.2021.113922.

[5] M. Kumar, A. M. Sidpara and V. Racherla. 2022. Surface finishing of aluminium 6061 using fabricated flexible abrasive tool. Mater. Today Commun. 33: 104614, doi: 10.1016/j.mtcomm.2022.104614.

[6] A. Y. Nasution, M. R. M. Rejab, Q. Ma and M. A. Firmansyah. 2021. Design optimization of passenger SUV's crash box and bumper beam by using finite element method. IOP Conf. Ser. Mater. Sci. Eng., 1068(1): 012023, doi: 10.1088/1757-899x/1068/1/012023.

[7] H. Zhang, Z. Sun, M. Zhang, Y. Shao and J. Zhu. 2020. Comparison of the flow structures and regime transitions between a cylindrical fluidized bed and a square fluidized bed. Powder Technol., 376: 507-516, doi: 10.1016/j.powtec.2020.08.072.

[8] S. Wesselmecking, M. Kreins, M. Dahmen and W. Bleck. 2022. Material oriented crash-box design - Combining structural and material design todoc_improve specific energy absorption. Mater. Des. 213: 110357, doi: 10.1016/j.matdes.2021.110357.

[9] M. Yang *et al*. 2021. Crashworthiness of hierarchical truncated conical shells with corrugated cores. Int. J. Mech. Sci., 193: 106171, doi: 10.1016/j.ijmecsci.2020.106171.

[10] T. Miguel Encarnação Nunes, A. Calado Marta Eng Luís Miguel Ouro Colaço, F. Szolnoky Ramos Pinto Cunha Supervisor and A. Calado Marta. 2017. Multi-objective design optimization of a frontal crash energy absorption system for a road-safe vehicle Aerospace Engineering Examination Committee. (November): 30-46.

[11] E. Raponi, M. Bujny, M. Olhofer, N. Aulig, S. Boria and F. Duddeck. 2019. Kriging-assisted topology optimization of crash structures. Comput. Methods

Appl. Mech. Eng., 348: 730-752, doi: 10.1016/j.cma.2019.02.002.

[12] J. Wang, Y. Zhang, N. He and C. H. Wang. 2018. Crashworthiness behavior of Koch fractal structures. Mater. Des. 144: 229-244, doi: 10.1016/j.matdes.2018.02.035.

[13] D. Frej and M. Jaskiewicz. 2021. Test Stand for Experimental Crash Tests at Low Speeds," Transp. Res. Procedia, 55: 1627-1634, doi: 10.1016/j.trpro.2021.07.152.

[14] Y. Song, M. V. Chitturi and D. A. Noyce. 2021. Automated vehicle crash sequences: Patterns and potential uses in safety testing. Accid. Anal. Prev., 153: 106017, doi: 10.1016/j.aap.2021.106017.

[15] G. Wang, Y. Zhang, Z. Zheng, H. Chen and J. Yu. 2022. Crashworthiness design and impact tests of aluminum foam-filled crash boxes. Thin-Walled Struct., vol. 180, doi: 10.1016/j.tws.2022.109937.

[16] A. Gudisey, J. Magliaro and W. Altenhof. 2021. High capacity, adaptive energy absorption under tensile loading conditions utilizing an axial cutting deformation mode. Forces Mech., vol. 2, doi: 10.1016/j.finmec.2020.100004.

[17] M. Quanjin, M. S. A. Salim, M. R. M. Rejab, O. E. Bernhardi and A. Y. Nasution. 2020. Quasi-static crushing response of square hybrid carbon/aramid tube for automotive crash box application. in Materials Today: Proceedings, 27: 683-690, doi: 10.1016/j.matpr.2019.10.161.

[18] J. Huang and K. J. Bathe. 2020. Overlapping finite element meshes in AMORE. Adv. Eng. Softw. vol. 144, doi: 10.1016/j.advengsoft.2020.102791.

[19] L. Guo, H. Huang, C. Jia and K. Romanov. 2020. Axial behavior of square CFST with local corrosion simulated by artificial notch. J. Constr. Steel Res., 174: 106314, doi: 10.1016/j.jcsr.2020.106314.

[20] M. Ferdynus, K. Szklarek and M. Kotełko. 2022. Crashworthiness performance of thin-walled hollow and foam-filled prismatic frusta, Part 2: Experimental study. Thin-Walled Struct., vol. 181, doi: 10.1016/j.tws.2022.110070.

[21] M. Rogala and J. Gajewski. 2023. Crashworthiness Analysis of Thin-Walled Square Columns with a Hole Trigger. Materials (Basel). 16(11), doi: 10.3390/ma16114196.

[22] T. Pang, G. Zheng, J. Fang, D. Ruan and G. Sun. 2019. Energy absorption mechanism of axially-varying thickness (AVT) multicell thin-walled structures under out-of-plane loading. Eng. Struct., 196: 109130, doi: 10.1016/j.engstruct.2019.04.074.

[23] B. Jiang *et al*. 2019. Numerical, theoretical, and experimental studies on the energy absorption of the thin-walled structures with bio-inspired constituent element. Int. J. Mech. Sci., 164(August): 105173, doi: 10.1016/j.ijmecsci.2019.105173.

[24] C. H. Zhou, B. Wang, H. Z. Luo, Y. W. Chen, Q. H. Zeng and S. Y. Zhu. 2017. Quasi-Static Axial Compression of Origami Crash Boxes. Int. J. Appl. Mech., 9(5): 1750066, doi: 10.1142/S1758825117500661.

[25] K. Maier, T. Klünsner, M. Krobath, C. Tritremmel, S. Marsoner and C. Czettl. 2020. Uniaxial step loading test setup for determination of creep curves of oxidation-sensitive high strength materials in vacuum under tensile and compressive load. Int. J. Refract. Met. Hard Mater. 92: 105327, doi: 10.1016/j.ijrmhm.2020.105327.

[26] T. Sonar, M. Ivanov, E. Trofimov, A. Tingaev and I. Suleymanova. 2023. A comprehensive review on fusion welding of high entropy alloys - Processing, microstructural evolution and mechanical properties of joints. Int. J. Light. Mater. Manuf., 7(1): 122-183, doi: 10.1016/j.ijlmm.2023.06.003.

[27] İ. Özen, H. Gedikli and M. Aslan. 2023. Experimental and numerical investigation on energy absorbing characteristics of empty and cellular filled composite crash boxes. Eng. Struct., 289: 116315, doi: 10.1016/j.engstruct.2023.116315.

[28] A. Singh, V. Singh, A. P. Singh, D. Patel and S. K. Gupta. 2023. Experiment analysis of A-TIG welding and comparison between TIG, Double-TIG, and A-TIG of Hastelloy C-276. Mater. Today Proc., doi: 10.1016/j.matpr.2023.05.199.

[29] M. Harhash, M. Kuhtz, J. Richter, A. Hornig, M. Gude, and H. Palkowski. 2021. Trigger geometry influencing the failure modes in steel/polymer/steel sandwich crashboxes: Experimental and numerical evaluation.

Compos. Struct. 262: 113619, doi: 10.1016/j.compstruct.2021.113619.

[30] O. M. Qureshi and E. Bertocchi. 2013. Crash performance of notch triggers and variable frequency progressive-triggers on patterned box beams during axial impacts. Thin-Walled Struct. 63: 98-105, doi: 10.1016/j.tws.2012.07.021.

[31] S. Boria. 2017. Crashworthiness optimization of an automotive front bumper. Proc. 7th Int. Conf. Coupled Probl. Sci. Eng. COUPLED Probl. 2017, 2017-Janua: 835-846.

[32] D. Rajak and P. Patil. 2019. Modular Hybrid Crash Box Comprising with Helical Compression Spring and Metal Foam.

[33] Z. Li, Q. Yu, X. Zhao, M. Yu, P. Shi and C. Yan. 2017. Crashworthiness and lightweight optimization to applied multiple materials and foam-filled front end structure of auto-body. Adv. Mech. Eng. 9(8): 1-21, doi: 10.1177/1687814017702806.